Dielectric matrix calculation of the differential cross section for plasmon excitation and application to electron diffraction

T. W. Josefsson, R. L. Cobal, and L. J. Allen
School of Physics, University of Melbourne, Parkville, Victoria 3052, Australia
(Received 29 February 1996; revised manuscript received 4 June 1996)

We present a calculation of the differential cross section for plasmon excitation in Si based on a dielectric matrix which takes into account the electronic band structure of the solid. This result is compared with simple free-electron theory. The differential cross sections are then applied to calculate energy unfiltered convergent beam electron-diffraction patterns for Si for cases where experimental data exist. The simple model for multiple scattering due to plasmon excitation used here gives good overall agreement with experiment, the dielectric matrix calculation more so than that using free-electron theory. [S0163-1829(96)05841-9]

I. INTRODUCTION

The effects of single-particle or collective electronic (plasmon) excitations play a significant role in quantitative electron diffraction and microscopy. These excitations of states in the electron band structure of the solid are generally associated with energy losses of the order of 1–50 eV and relatively small momentum transfer.[1] This compares with the relatively small energy losses (of the order of meV),[2,3] and large momentum transfers involved in phonon excitation leading to thermal-diffuse scattering (TDS). Energy filters may therefore be used to exclude scattered electrons that have induced electronic excitations. However, in energy unfiltered experiments these electrons often (in all but the thinnest of crystals) contribute the majority of the scattered electron intensity. Dielectric response theory is a formalism convenient for describing the interaction between the incident electron and electronic states in the solid leading to plasmon excitations, and has been used to calculate the cross section for plasmon excitation using various approximations.[4] Because of the highly delocalized nature of the crystal states involved in plasmon excitations, simple free-electron theory was often used successfully.[4] In this work we present a model for the differential cross section for plasmon excitation in terms of the dielectric response matrix of the solid. We calculate the differential cross section for plasmon excitation in Si using this model. The random-phase approximation dielectric matrix is based on a realistic electronic band structure (calculated using a nonlocal empirical pseudopotential), and has been used successfully to calculate inelastic mean free paths.[5,6]

Electron-diffraction and microscopy experiments employing energy filtering can yield an abundance of structural information about various crystals.[7–9] In particular, quantitative analysis of energy filtered convergent beam electron-diffraction (CBED) patterns is used to determine crystal structure factors, specimen thicknesses, unit-cell parameters, charge-density distributions, and symmetries.[7,8,10] However, in some situations the use of energy filters is neither desirable[11,12] nor convenient.[13,14] The effects of plasmon excitation in energy unfiltered electron-diffraction and microscopy experiments, although known to be significant, are difficult to model quantitatively. This is due to both the kinematics of the plasmon excitation process and the dominance of multiple-scattering processes over single events, the more so the thicker the crystal. A number of models exist to simulate the effects of multiple scattering due to plasmon excitation in crystals, all of which require in effect some knowledge of the differential cross section for plasmon excitation. The method outlined in Ref. 15 (see also, Refs. 4 and 16) considers the effect of multiple scattering due to plasmon excitation via a simple convolution with the elastic intensity. We will use this model here to consider the effect of the differential cross section for plasmon excitation on the final intensity. A recently formulated multiple-scattering theory based on the kinetic equation (KE) for the one-particle density matrix[17] has shown that plasmon excitation leads both to the expected damping of coherence by small-angle scattering, and the asymmetry observed in certain energy unfiltered CBED intensity profiles.[11] However this theory, while being in good agreement with experiment is somewhat more complex to implement. In this work we compare the energy unfiltered Si CBED patterns and the KE calculation in Ref. 17 with the simple and computationally convenient multiple-scattering convolution method, which nevertheless utilizes no open parameters.

In Sec. II we outline the relationship between the differential cross section for plasmon excitation and the dielectric response matrix for a crystal. The differential cross sections calculated both from dielectric response theory and from free-electron theory are discussed. These cross sections are then used in the multiple-scattering convolution method to calculate Si CBED intensity patterns in Sec. III. We discuss the CBED intensity profile as calculated in this model, comparing the results with experiment and the more sophisticated multiple-scattering model based on the KE.

II. DIFFERENTIAL CROSS SECTION FOR PLASMON EXCITATION IN SILICON

A realistic representation of the cross section for plasmon excitation requires detailed consideration of the electronic structure of the solid. The valence electronic structure of a crystalline material consists of many electron energy states whose wave functions are associated with chemical bonding

effects,[9] making it difficult to treat individually the excitation of each state within the band. It is more convenient to introduce a dielectric response function $\epsilon(\mathbf{q},\omega)$ where $\mathbf{q}$ is the wave vector of the field and ω is the frequency, characterizing the statistical properties of valence and conduction electrons.[18] It follows trivially from Maxwell's equations that the existence of nonzero longitudinal fields corresponding to longitudinal charge-density oscillations (volume-plasmon excitations) in the bulk solid of wave vector $\mathbf{q}$ and frequency $\omega(\mathbf{q})$ requires $\varepsilon(\mathbf{q},\omega)=0$. Because $\varepsilon(\mathbf{q},\omega)$ is complex this criterion is observed experimentally by maxima in the dielectric loss function[4] $-\mathrm{Im}[1/\varepsilon(\mathbf{q},\omega)]$. However, due to the discrete translational symmetry of the crystal lattice, an external field of frequency ω and wave vector $\mathbf{q}$ gives rise to many rapidly oscillating microscopic fields of frequency ω and wave vector $\mathbf{q}+\mathbf{g}$, where $\mathbf{g}$ is a reciprocal-lattice vector. This results in a matrix formulation of the dielectric function, relating the displacement field and the microscopic fields by $D(\mathbf{q}+\mathbf{g},\omega)=\Sigma_{\mathbf{h}}\varepsilon_{\mathbf{g},\mathbf{h}}(\mathbf{q},\omega)E(\mathbf{q}+\mathbf{h},\omega)$. The existence of nonzero microscopic longitudinal fields now requires $\det|\varepsilon_{\mathbf{g},\mathbf{h}}(\mathbf{q},\omega)|=0$. The observable macroscopic dielectric function is then obtained from the reciprocal of the first element in the inverse microscopic dielectric matrix $\epsilon(\mathbf{q},\omega)=1/[\epsilon^{-1}_{0,0}(\mathbf{q},\omega)]$. This allows a realistic representation of the dielectric response over a large range of frequencies and wave vectors to be obtained. The inclusion of these microscopic or local field effects is well known to have a dramatic effect on $\varepsilon(\mathbf{q},\omega)$ and in particular the loss function.[5,6]

In the dielectric response formalism, the total cross section (per unit volume) for plasmon excitation may be written as[5]

$$\sigma=-\frac{8\pi e^2 m}{\hbar^2 K}\int_0^{E_0/\hbar}d\omega\int_{-\mathbf{q}_{\max}}^{\mathbf{q}_{\max}}\frac{d\mathbf{q}}{(2\pi)^3}\frac{1}{q^2}\mathrm{Im}\left[\frac{-1}{\epsilon(\mathbf{q},\omega)}\right]\times\delta\left(\omega-\mathbf{q}\cdot\mathbf{v}+\frac{\hbar q^2}{2m}\right),\tag{2.1}$$

for an incident electron of energy E_0 (with wave vector K) and velocity $\mathbf{v}$. The integration is over all possible momentum transfers $\hbar\mathbf{q}$ consistent with an energy loss of $\hbar\omega$. Assuming dielectric isotropy (a good approximation for most solids), $\epsilon(\mathbf{q},\omega)\approx\epsilon(q,\omega)$ and transformation to polar coordinates $d\Omega=\sin\theta d\theta d\phi$ enables us to obtain the differential cross section (per unit volume) for plasmon excitation as

$$\frac{\partial\sigma(\theta)}{\partial\Omega}=-\frac{8\pi e^2 m}{\hbar^2 K}\int_0^{E_0/\hbar}d\omega\int_0^{q_{\max}}\frac{dq}{(2\pi)^3}\mathrm{Im}\left[\frac{-1}{\epsilon(q,\omega)}\right]\times\delta\left(\omega-qv\cos\theta+\frac{\hbar q^2}{2m}\right).\tag{2.2}$$

The mean free path Λ $(=1/\sigma)$ can then easily be shown to reduce to the well-known Pines[19] and Howie[20] result for an isotropic crystal.

In order to calculate the differential cross section we require the dielectric loss function obtained from the inversion of the dielectric matrix. In the random-phase approximation the dielectric matrix may be written as[21,22]

$$\epsilon_{\mathbf{g},\mathbf{h}}(\mathbf{q},\omega)=\delta_{\mathbf{h},\mathbf{g}}-\frac{4\pi e^2}{NV_c|\mathbf{q}+\mathbf{g}||\mathbf{q}+\mathbf{h}|}\lim_{\alpha\to 0^+}\sum_{\mathbf{k},n,n'}\frac{f_0[E_{n'}(\mathbf{k}+\mathbf{q})]-f_0[E_n(\mathbf{k})]}{E_{n'}(\mathbf{k}+\mathbf{q})-E_n(\mathbf{k})+\hbar\omega+i\hbar\alpha}\times\langle\mathbf{k}+\mathbf{q},n'|e^{i(\mathbf{q}+\mathbf{g})\cdot\mathbf{r}}|\mathbf{k},n\rangle\langle\mathbf{k},n|e^{-i(\mathbf{q}+\mathbf{h})\cdot\mathbf{r}}|\mathbf{k}+\mathbf{q},n'\rangle.\tag{2.3}$$

Here $f_0(E)$ is the Fermi distribution for the energy E, while α is the inverse lifetime of a single-particle excitation and NV_c is the volume of the crystal. The Brillouin-zone summation $\Sigma_{\mathbf{k},n,n'}$ is over all possible transitions between the states $|\mathbf{k},n\rangle$ of energy $E_n(\mathbf{k})$ and $|\mathbf{k}+\mathbf{q},n'\rangle$ of energy $E_{n'}(\mathbf{k}+\mathbf{q})$. In order to evaluate the dielectric matrix for Si a nonlocal empirical psuedopotential band structure[23–25] was used to calculate the four highest valence and 30 lowest conduction states as required in the summation over crystal states. The simple psuedopotential method lends itself to fast and efficient calculations of an accurate band structure and is therefore well suited for this application. The Brillouin-zone summation extended over a minimum of 182 $\mathbf{k}$ points (selected via the special-points scheme of Ref. 26) in the irreducible Brillouin zone, using the analytic integration technique of Ref. 27. Great care was taken to ensure numerical convergence[25,28,29] before the full 59×59 dielectric matrix was inverted for each frequency ω and q point to obtain the loss function.[6]

In Fig. 1 we show the differential cross section for plasmon excitation in Si as a function of incident energy calculated according to dielectric response theory [using Eq. (2.2)]. The results are shown on a linear scale in Fig. 1(a) and on a log-log plot in Fig. 1(b) due to the wide variation in the differential cross section as a function of angle and incident energy. Because of the widespread use of the simple free-electron model (and variations thereof[4,30,31]), it is instructive to compare the dielectric matrix results with those obtained from a free-electron model. In free-electron theory the differential cross section is Lorentzian as a function of scattering angle θ,

$$\frac{\partial\sigma(\theta)}{\partial\Omega}\propto\frac{1}{\theta_E^2+\theta^2}.\tag{2.4}$$

The full width at half maximum (FWHM) of the free-electron cross section is given by $2\theta_E=\hbar\omega_p/E_0$ and the plasmon energy by $\hbar\omega_p=\sqrt{\hbar^2 e^2 n_0/m_0\epsilon}$, where n_0 is the electron plasma density. Because the free-electron result is Lorentzian, we may expect that the differential cross section as calculated from Eq. (2.2) is also approximately Lorentzian

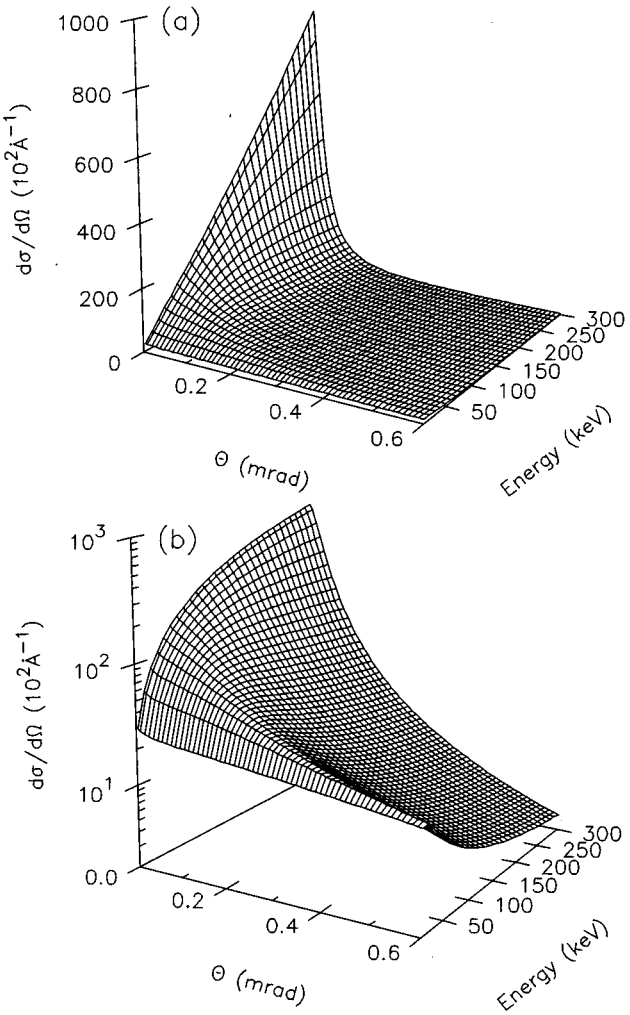

FIG. 1. (a) The differential cross section (per unit volume) for plasmon excitation in Si as a function of incident electron energy. (b) The results in (a) on a log-log plot. The results are obtained from inversion of dielectric matrices of order 59×59, based on a nonlocal empirical psuedopotential band structure.

as a function of scattering angle θ. This is indeed the case, as can be seen in Figs. 2(a) and 2(b) for an energy (chosen to facilitate comparison with experiment in the next section) of 80 keV. The dielectric response matrix calculation of the differential cross section falls off more rapidly than a Lorentzian at high angles. This effect has been seen experimentally[4] for Al and is due to the dominance of single-electron excitations over collective energy losses, as high momentum plasmons become poorly defined elementary excitations in the solid.[16]

The free-electron FWHM of $\Gamma=0.207$ mrad at 80.0 keV yields $\Lambda=1140$ Å. This compares with the dielectric response matrix calculation which yields $\Gamma=0.201$ mrad and $\Lambda=894$ Å. The experimentally determined values of the mean free path vary over a sizeable range. For an incident electron of energy 80 keV in Si, the experimentally observed result is approximately $600-1000$ Å.[4,5] The dielectric matrix based result lies within this range, but the free-electron result slightly overestimates the mean free path.

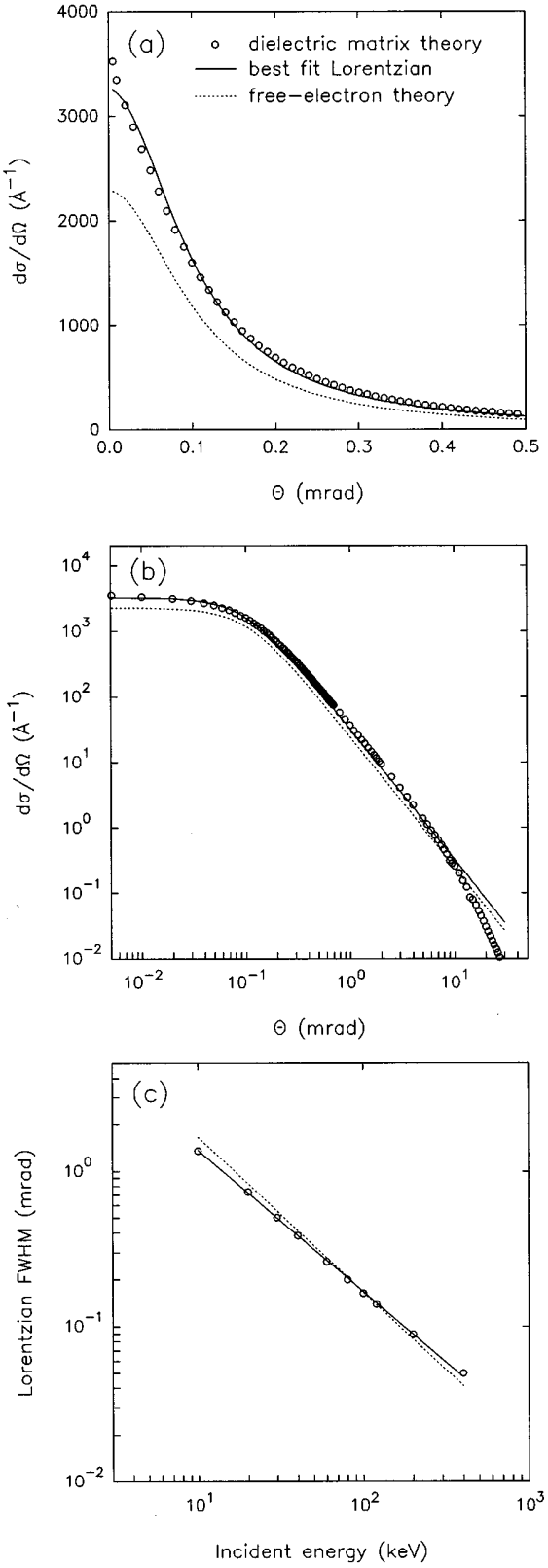

FIG. 2. (a) The differential cross section (per unit volume) for plasmon excitation in Si for 80 keV incident electrons. Results calculated from dielectric matrix theory are compared with the best fit Lorentzian distribution (with FWHM=0.201 mrad) and free-electron results. (b) The differential cross section over a greater range shown on a log-log plot. (c) The FWHM of the differential cross section calculated for a range of incident energies on a log-log plot.

TABLE I. The mean free path (Λ) and Lorentzian FWHM (Γ) as a function of incident energy calculated from dielectric response theory (DRT) and free-electron theory (FET).

E_0 (keV)	20.0	40.0	60.0	80.0	100.0	120.0	150.0	200.0	300.0	400.0
Λ DRT (Å)	324	543	730	894	1040	1170	1341	1580	1935	2164
Λ FET (Å)	343	625	889	1140	1385	1623	1969	2525	3584	4594
Γ DRT (mrad)	0.735	0.384	0.262	0.201	0.164	0.139	0.114	0.089	0.063	0.050
Γ FET (mrad)	0.830	0.415	0.277	0.208	0.166	0.139	0.111	0.083	0.055	0.042

The calculated results have been fitted with Lorentzian distributions whose FWHM (Γ) as a function of incident energy are shown in Table I, along with the mean free path obtained from integration of the differential cross sections. The results obtained from free-electron theory are also shown in the table. The FWHM decreases with electron energy as scattering due to plasmon excitation becomes increasingly concentrated over a small angular range. This behavior of the FWHM is linear as a function of incident energy when represented on a log-log plot, as in Fig. 2(c).

III. ENERGY UNFILTERED CBED INTENSITY PROFILES FOR SILICON

In many high-energy electron-diffraction and microscopy experiments, fast electrons propagate through the crystal for distances comparable to or greater than the mean free path for plasmon excitation, so that multiple-scattering effects must be considered from the outset. The multiple-scattering model of Dudarev *et al.*[17] which includes the effects of dynamical scattering of the inelastic electrons may be used for this purpose. However, for utilitarian purposes, a simpler and computationally convenient model has been developed and used recently in Ref. 15.

For high-energy transmission electron diffraction the intensity profile $I(\mathbf{g},t,\theta,\phi)$ of electrons having undergone elastic and multiple-scattering due to plasmon excitation to the position specified by θ and ϕ, in the **g**th beam and for a crystal of thickness t, may be written as

$$I(\mathbf{g},t,\theta,\phi)=\lim_{N\to\infty}\sum_{n=0}^{N}P_n(t)I_n(\mathbf{g},t,\theta,\phi). \tag{3.1}$$

The $I_n(\mathbf{g},t,\theta,\phi)$ are obtained using the recurrence relation

$$I_n(\mathbf{g},t,\theta,\phi)=\frac{1}{\sigma}\int I_{n-1}(\mathbf{g},t,\theta'-\theta,\phi'-\phi)\frac{\partial\sigma(\theta')}{\partial\Omega'}d\Omega', \tag{3.2}$$

where $P_n(t)=(1/n!)(t/\Lambda)^n e^{-t/\Lambda}$ is the probability of an electron exciting a plasmon n times after traversing a distance t in the crystal. The simplicity and utility of this model (which is equivalent to that used in Ref. 15) lies in the fact that only the form of the differential cross section for plasmon excitation and the routinely calculated elastic scattered intensity $I_0(\mathbf{g},t,\theta,\phi)$ are required. The differential cross section may in turn be obtained from theory, whether it be a sophisticated dielectric response matrix calculation as in Sec. II or simple free-electron theory, or from experiment.

We apply this simple multiple-scattering method to the energy unfiltered CBED data of Dudarev *et al.*[11,17] In this experiment 80 keV electrons are incident on Si crystals of thickness 2340, 2860, and 3420 Å at $T=100$ K for the $\{110\}$ systematic row orientation. The axis of the convergent beam is offset by a Bragg angle so that (220) is in the exact Bragg orientation with respect to the axis of the convergent beam. However, the convergent beam was set to span only one Bragg angle θ_B, instead of the usual $2\theta_B$ for a CBED pattern. This was done in order to minimize any inelastic intensity ''leakage'' between beams that would be quite apparent in the usual CBED geometry where the beams lie exactly adjacent to each other. Theoretical CBED intensity profiles have been obtained by calculating the intensity associated with each of the four lowest-order central disks in the CBED pattern obtained from an 11-beam Bloch wave calculation. Absorption from the elastic intensity due to TDS was included using the Einstein model[32] with a Debye-Waller factor obtained using a projected mean-square displacement of $\langle u^2\rangle=0.0029$ Å^2. The Bloch wave calculation was performed following the method described in Refs. 33 and 34. The intensity of each of these disks [$(\bar{2}\bar{2}0)$, (000), (220), (440)] was used as the intitial $I_0(\mathbf{g},t,\theta,\phi)$ in Eq. (3.2), to obtain the final intensity profile using Eq. (3.1). The number of multiple-scattering orders (N) considered for a given thickness was chosen by requiring the probability $\Sigma_{n=0}^{N}P_n(t)$ to be at least 99.9% of the result obtained for the case $N\to\infty$. For the thicknesses considered in this work, typically $N=8$. The intensity of TDS scattered electrons was assumed to contribute an approximately constant orientation independent term (as discussed in Ref. 11) and is not shown in these calculated CBED images. In practice the experimental CBED image will also contain Kikuchi lines formed by diffraction of large angle inelastic scattered electrons [mainly due to TDS (Ref. 35)]. This effect is more significant for thicker crystals at higher temperatures due to the increased amount of TDS, but its mathematical modeling remains difficult.[9]

In Fig. 3(a) we show the simulated energy unfiltered intensity profile for the central (000) (on the left) and the (220) CBED disks. We note that the intensity of both the $(\bar{2}\bar{2}0)$ and the (440) CBED disks are very weak and so are not shown. The corresponding energy filtered results are shown below in Fig. 3(b). Figure 4 shows the calculated energy unfiltered [Fig. 4(a)] and energy filtered [Fig. 4(b)] (220) disk, exposed to bring out the detail washed out by the bright central (000) disk in Fig. 3. It is clear from reference to Fig. 4(b) that the elastic or energy filtered (220) CBED disk is symmetrical in intensity about the center of the disk. As can be seen from Fig. 4(a) the energy unfiltered (220) CBED disk shows only a marginal increased intensity on the (left) side nearest the bright central (000) disk compared

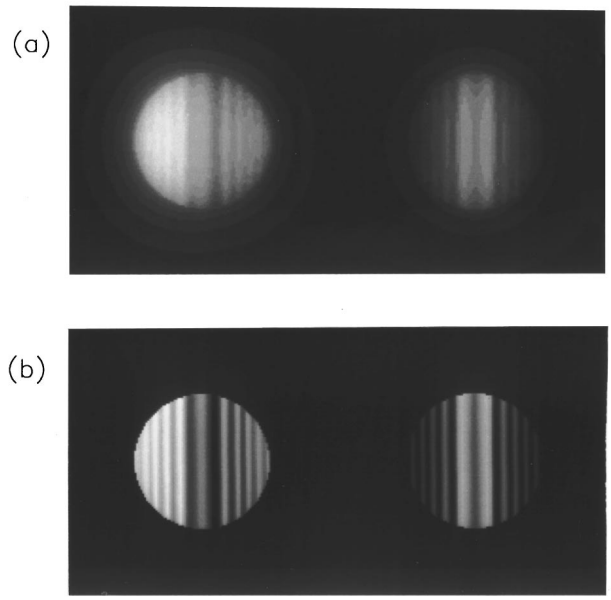

FIG. 3. The calculated (000) (on the left) and (220) CBED disks for 80 keV electrons incident on a 2860 Å thick Si crystal. The incident beam axis is tilted by a Bragg angle from the crystal normal. (a) The energy unfiltered (elastic plus plasmon scattered) CBED intensity profile. (b) The energy filtered (elastic) intensity profile calculated without including the effects of small-angle scattering away from the elastic beams.

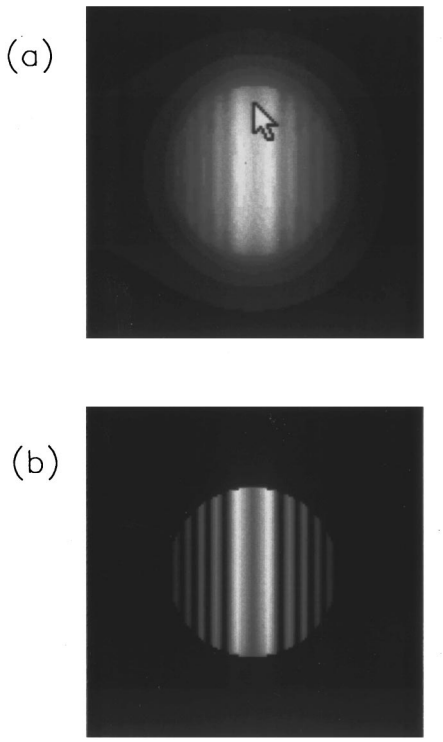

FIG. 4. The calculated (220) CBED disk in Fig. 3 exposed to show details ''washed out'' by the bright (000) disk in Fig. 3. (a) The energy unfiltered (elastic plus plasmon scattered) CBED intensity profile. This result can be compared with the experimental results of Fig. 2 in Dudarev *et al.* (Ref. 17). (b) The energy filtered (elastic) intensity profile. The decrease in intensity along the vertical axis from the center of the disk (see arrow) is clearly visible in the energy unfiltered case, but is of course not seen in the energy filtered case.

with the other side nearest the (440) disk. This intensity variation is due to multiple small-angle inelastic scattering from the much brighter (000) disk into the (220) disk and would be more pronounced if a CBED scan spanning a convergence angle of $2\theta_B$ was used.

A direct comparison of the experimental CBED pattern shown in Fig. 2 of Ref. 17 can be made with the theoretical result shown in Fig. 4(a) of this work. The multiple-scattering convolution method can be seen to result in good agreement with experiment. A detailed comparison of the experimental data with the kinetic equation calculation of Dudarev *et al.*[17] and the multiple-scattering model used in this work may be found in Fig. 5 for a Si crystal of thicknesses 2340 Å [Fig. 5(a)], 2860 Å [Fig. 5(b)], and 3420 Å [Fig. 5(c)], respectively. The numerical solution of the kinetic equation for the one-particle density matrix[17] (taking multiple scattering due to plasmon excitation into account implicitly) is seen to reproduce the asymmetrical trend displayed by the experimental intensity profiles. In comparison, the multiple-scattering convolution method used in this work shows very little asymmetry. This is due to the neglect of dynamical effects such as resonance errors in the treatment of multiple plasmon scattering as a simple multiple convolution of the final quasielastic intensity with the differential cross section for plasmon excitation.

A somewhat smaller intensity contrast in the energy unfiltered profiles would appear desirable in all cases for our calculations. This suggests a slightly smaller elastic intensity profile and hence a smaller mean free path for plasmon excitation. This could be due to an underestimation of the differential cross section for plasmon excitation, and hence an overestimation of the mean free path, obtained from the dielectric response matrix. A mean free path smaller (but still within experimental uncertainty) than our calculated result could account for this. This is consistent with the fact that most theoretical calculations of the mean free path (including, albeit to a lesser degree, the dielectric matrix calculation of this work) tend to understate the total number of single-particle excitations and transitions that can occur in a real solid. This results in an overstated mean free path.

In Fig. 6 we compare the experimental energy unfiltered intensity profiles (solid lines) with the calculated results based on the dielectric response matrix calculation of the differential cross section for plasmon excitation (dotted line) and free-electron theory (broken line) for the same conditions as in Fig. 5. The dielectric response matrix mean free path (894 Å) is shorter than the free-electron mean free path (1140 Å) and gives better agreement with experiment. We stress that care should be taken when considering fine detail in the CBED profiles calculated by the multiple-scattering convolution method outlined in this work. It is a convenient but approximate model for the complex multiple-scattering mechanisms occurring in the solid. Nonetheless, the model yields reasonable agreement with experiment when using the dielectric matrix based differential cross section. However, the results indicate that there is a noticeable sensitivity to the differential cross section for plasmon excitation used to obtain the final intensity patterns. The use of simple free-electron models may induce (depending on the incident elec-

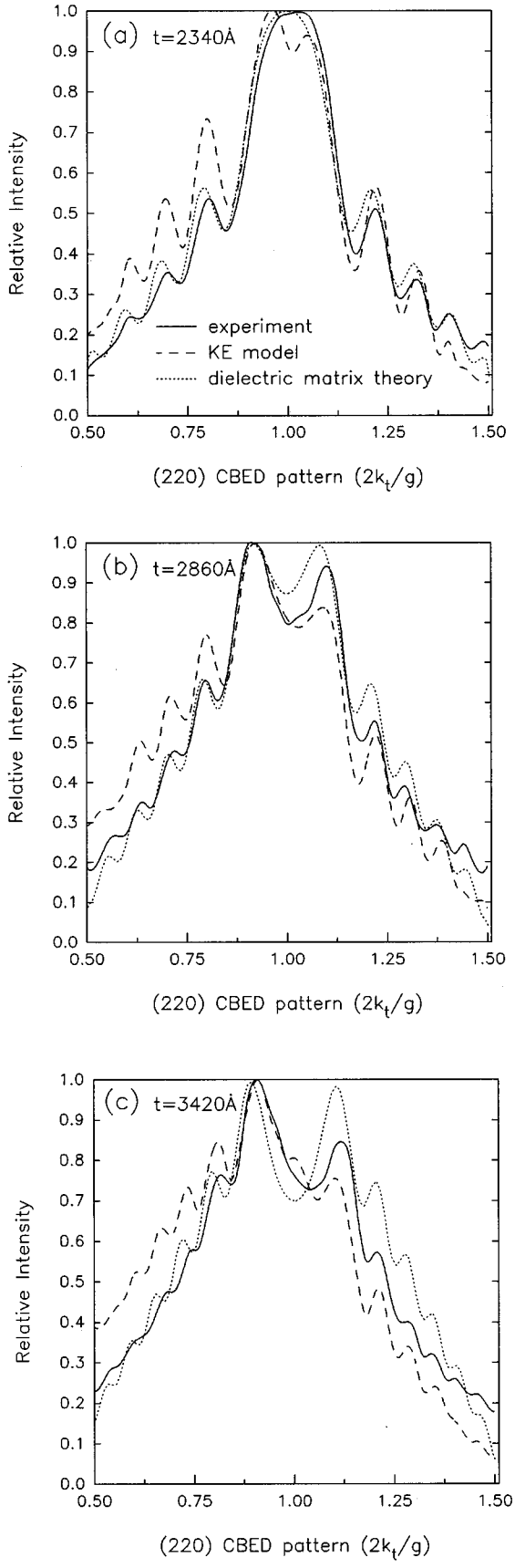

FIG. 5. The (220) CBED intensity profile for 80 keV electrons incident on Si of thickness (a) 2340 Å, (b) 2860 Å, and (c) 3420 Å. The dielectric matrix results are compared with the experimental results and KE model of Dudarev *et al.* (Ref. 17).

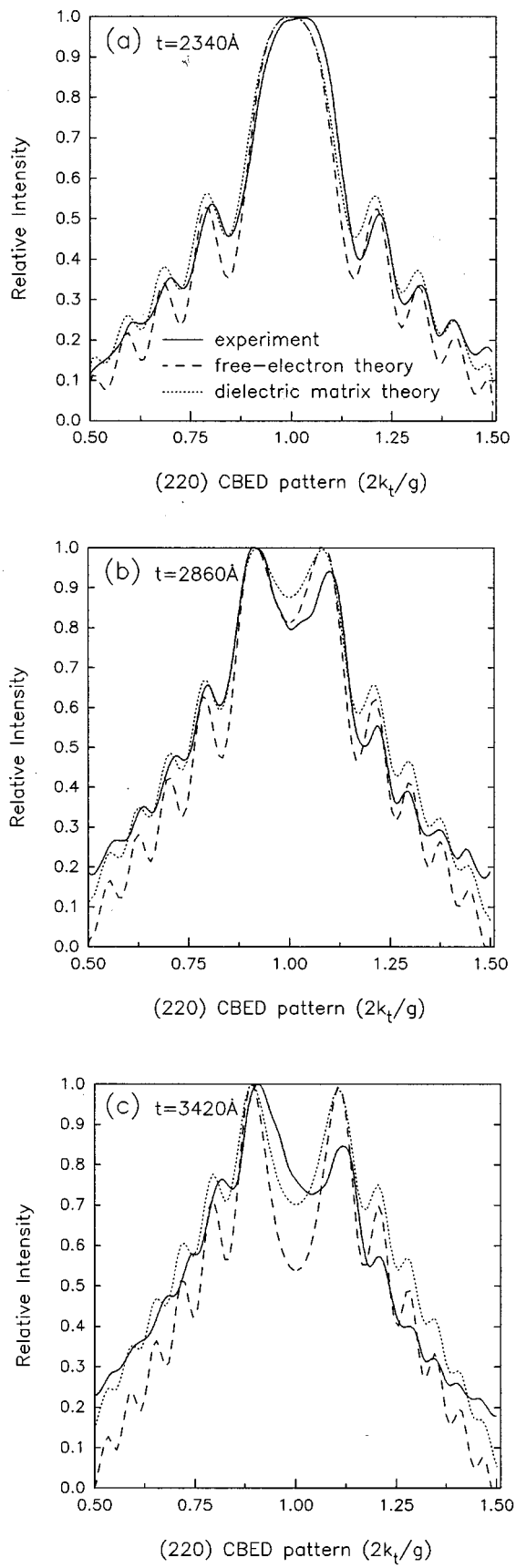

FIG. 6. The (220) CBED intensity profiles for 80 keV electrons incident on Si of thickness (a) 2340 Å, (b) 2860 Å, and (c) 3420 Å. The dielectric matrix and free-electron theory results are compared with the experimental results of Dudarev *et al.* (Ref. 17).

tron energy) errors in the final intensity which negate benefits gained from using a more accurate multiple-scattering model.

IV. CONCLUSIONS

A first-principles calculation of the differential cross section for plasmon excitation in Si has been performed, based on an electronic band-structure-dependent dielectric matrix calculation. The differential cross section was found to be more delocalized at higher incident energies (100 keV), and more localized at lower energies, than simple free-electron models indicate. The result was applied in a simple model using dynamical Bloch wave theory to simulate the effects of multiple-scattering due to plasmon excitation in energy unfiltered convergent beam electron diffraction. Results based on the first-principles dielectric matrix calculation of the differential scattering cross section due to plasmon excitation were found to compare favorably both with experiment and a recently formulated multiple-scattering theory based on the kinetic equation for the one-particle density matrix. The sensitivity of the intensity patterns to the particular differential cross section used indicates that care should be taken when analyzing results using free-electron theory.

ACKNOWLEDGMENTS

The authors would like to thank Dr. A. E. C. Spargo for helpful discussions in the course of completing this work and Dr. S. L. Dudarev for supplying in digital form the experimental and theoretical KE data from Ref. 17 used in Figs. 5 and 6. L.J.A acknowledges financial support from the Australian Research Council.

[1] C. J. Rossouw and M. J. Whelan, Ultramicroscopy, **6**, 53 (1981).
[2] C. R. Hall and P. B. Hirsch, Proc. R. Soc. London Ser. A **286**, 158 (1965).
[3] C. J. Humphreys and P. B. Hirsch, Philos. Mag. **18**, 115 (1968).
[4] H. Raether, in *Excitation of Plasmons and Interband Transitions by Electrons*, edited by G. Höhler, Springer Tracts in Modern Physics, Vol. 88 (Springer-Verlag, New York, 1980).
[5] T. W. Josefsson and A. E. Smith, Phys. Rev. B **50**, 7322 (1994).
[6] T. W. Josefsson and A. E. Smith, Phys. Lett. A **180**, 174 (1993).
[7] J. C. H. Spence and J. M. Zuo, *Electron Microdiffraction* (Plenum, New York, 1992).
[8] *Electron Diffraction Techniques*, edited by J. M. Cowley (Oxford University Press, Oxford, 1993).
[9] Z. L. Wang, *Elastic and Inelastic Scattering in Electron Diffraction and Imaging* (Plenum, New York, 1995).
[10] J. C. H. Spence, Acta Crystallogr. A **49**, 231 (1993).
[11] L. M. Peng, S. L. Dudarev, and M. J. Whelan, Phys. Lett. A **175**, 461 (1993).
[12] J. T. Czernuszka, N. J. Long, E. D. Boyes, and P. B. Hirsch, Philos. Mag. Lett. **62**, 227 (1990).
[13] J. M. McCoy, U. Korte, P. Maksym, and G. Meyer-Ehmsen, Surf. Sci. **261**, 29 (1992).
[14] G. Lehmpfuhl, D. Krahl, and Y. Uchida, Acta Crystallogr. A **51**, 504 (1995).
[15] K. Marthinsen, R. Holmestad, and R. Hoier, Ultramicroscopy **55**, 268 (1994).
[16] R. F. Egerton and K. Wong, Ultramicroscopy **59**, 169 (1995).
[17] S. L. Dudarev, L. M. Peng, and M. J. Whelan, Phys. Rev. B **48**, 13 408 (1993).
[18] R. H. Ritchie, Phys. Rev. **106**, 874 (1957).
[19] D. Pines, *Elementary Excitations in Solids* (Benjamin, New York, 1960).
[20] R. H. Ritchie and A. Howie, Philos. Mag. **36**, 463 (1977).
[21] S. Adler, Phys. Rev. **126**, 413 (1962).
[22] N. Wiser, Phys. Rev. **129**, 62 (1963).
[23] J. R. Chelikowsky and M. L. Cohen, Phys. Rev. B **14**, 559 (1976).
[24] M. L. Cohen and J. R. Chelikowsky, *Electronic structure and Optical Properties of Semiconductors* (Springer-Verlag, Berlin, 1989).
[25] T. W. Josefsson and A. E. Smith, Aust. J. Phys. **46**, 635 (1993).
[26] H. J. Monkhurst and J. D. Pack, Phys. Rev. B **13**, 518 (1976).
[27] N. W. Dalton and G. Gilat, Solid State Commun. **10**, 287 (1972).
[28] R. Daling, W. Van Haeringen, and B. Farid, Phys. Rev. B **45**, 8970 (1992).
[29] R. Daling, W. Van Haeringen, and B. Farid, Phys. Rev. B **44**, 2952 (1991).
[30] G. Radi, Acta Crystallogr. A **26**, 41 (1970).
[31] R. A. Ferrel, Phys. Rev. **101**, 554 (1956).
[32] M. J. Whelan, J. Appl. Phys. **36**, 2099 (1965).
[33] L. J. Allen and C. J. Rossouw, Phys. Rev. B **39**, 8313 (1989).
[34] T. W. Josefsson, L. J. Allen, P. R. Miller, and C. J. Rossouw, Phys. Rev. B **50**, 6685 (1994).
[35] L. J. Allen, C. J. Rossouw, and A. G. Wright, Ultramicroscopy **40**, 109 (1992).